Journal of Alloys and Compounds 480 (2009) 750–755

Contents lists available at ScienceDirect

Journal of Alloys and Compounds

journal homepage: www.elsevier.com/locate/jallcom

Electrochemical hydrogen storage characteristics of nanocrystalline and amorphous $Mg_{20}Ni_{10-x}Co_x$ ($x = 0$–4) alloys prepared by melt spinning

Yang-huan Zhang[a,b,*], Hui-ping Ren[b], Shi-hai Guo[a], Zai-guang Pang[b], Yan Qi[a], Xin-lin Wang[a]

[a] Department of Functional Material Research, Central Iron and Steel Research Institute, Beijing 100081, China
[b] School of Material, Inner Mongolia University of Science and Technology, Baotou 014010, China

ARTICLE INFO

Article history:
Received 5 January 2009
Received in revised form 9 February 2009
Accepted 10 February 2009
Available online 23 February 2009

Keywords:
Mg_2Ni-type electrode alloy
Melt-spinning
Structure
Electrochemical hydrogen storage

ABSTRACT

Nanocrystalline and amorphous Mg_2Ni-type electrode alloys with nominal compositions of $Mg_{20}Ni_{10-x}Co_x$ ($x = 0$, 1, 2, 3, 4) were synthesized by melt-spinning technique. The microstructures of the as-spun alloy ribbons were characterized by XRD, SEM and HRTEM. The electrochemical properties of the alloys were measured. The experimental results showed that the substitution of Co for Ni did not change the major phase of Mg_2Ni, but it led to the formation of secondary phase $MgCo_2$. No amorphous phase formed in the as-spun alloy ($x = 0$), whereas the as-spun alloy ($x = 4$) held a nanocrystalline and amorphous structure, confirming that the substitution of Co for Ni significantly enhances the glass forming ability of the Mg_2Ni-type alloy. The substitution of Co for Ni significantly improves the electrochemical hydrogen storage performances of the alloys, involving both the discharge capacity and the cycle stability, for which the increased glass forming ability by Co substitution is mainly responsible.

1. Introduction

Mg-based (Mg_2Ni-type) hydrogen storage alloys have attracted considerable interest in the last few years as hydrogen storage materials due to their major advantages such as high H/M ratio, low specific weight and low cost. However, some disadvantages of the Mg_2Ni-type electrode, sluggish hydriding/dehydriding kinetics and low electrochemical discharge capacity at room temperature, low diffusion rate of hydrogen, easy oxidation in alkaline solution, etc, make them still far from practical applications. Various attempts, particularly mechanical alloying (MA) [1], surface modification [2], and alloying with other elements [3], have been undertaken to improve the activation and hydriding properties.

Lei et al. obtained improved discharge capacities of around 500 mAh/g for Mg_2Ni alloys prepared by mechanical alloying (MA) at a current density of 20 mA/g [4]. Iwakura et al. [5] have also improved the discharge capacity of Mg-based alloy with graphite surface modification by mechanical grinding (MG). After surface modification with Ni powder by ball milling, Kohno and Kanda [6] have obtained a large discharge capacity of 750 mAh/g at a current density of 20 mA/g for modified Mg_2Ni alloys.

Although great efforts have been devoted to improve hydriding properties of the Mg–Ni-based alloys by manipulating their microstructures, MA Mg-based alloys showed extremely poor electrochemical cycle stability [7]. The MA/MG process has some insurmountable disadvantages such as the necessity of long time to produce an amorphous alloy, difficulty for mass-production, and contamination from the chamber and balls used in ball milling. Alternatively, the melt-spinning technique is the most useful method to obtain an amorphous and/or nanocrystalline phase in the absence of disadvantages inherent to the MA process and is more suitable for mass-production of amorphous alloys. Some advantageous of amorphous alloys, including high strength and toughness, excellent corrosion resistance, have been clarified by researchers in this field [8].

It was also expected that amorphous alloys produced by melt spinning could have excellent hydriding characteristics even at room temperature, similar to the alloys produced by the MA process. Huang et al. [9] found that amorphous and nanocrystalline Mg-based $(Mg_{60}Ni_{25})_{90}Nd_{10}$ alloy prepared by melt spinning obtained the highest discharge capacity of 580 mAh/g and the maximum hydrogen capacity of 4.2 wt.% H. Spassov and Köster [10] also reported that Mm (Mm = Ce, La-rich mischmetal) clearly increased the hydrogen absorption capacity of the melt-spun nanocrystalline/amorphous $Mg_{75}Ni_{20}Mm_5$ alloy. It was confirmed that an amorphous phase could be obtained in melt-spun Mg–Ni-based alloy by additive third element Pd, La and Ca [11]. Therefore, cobalt was chosen as the third element to obtain an amorphous phase in Mg_2Ni-type alloy by the melt-spinning technique. The objective of this work is to produce the Mg–Ni-based ternary nanocrystalline and amorphous alloys by melt spinning and to examine their electrochemical performances.

* Corresponding author at: Department of Functional Material Research, Central Iron and Steel Research Institute, 76 Xueyuan Nan Road, Haidian District, Beijing 100081, China. Tel.: +86 10 62187570; fax: +86 10 62184609.
E-mail address: zyh59@yahoo.com.cn (Y.-h. Zhang).

0925-8388/$ – see front matter © 2009 Elsevier B.V. All rights reserved.
doi:10.1016/j.jallcom.2009.02.039

2. Experimental

The alloy ingots were prepared using a vacuum induction furnace in a helium atmosphere with a pressure of 0.04 MPa in order to effectively prevent the volatilization of Mg. Part of the as-cast alloys was re-melted and spun with a rotating copper roller. The spinning rate was approximately expressed by the linear velocity of the copper roller because it is too difficult to measure a real spinning rate, i.e. cooling rate of the sample during spinning. The spinning rates used in the experiment were 15, 20, 25 and 30 m/s. The nominal compositions of the experimental alloys were $Mg_{20}Ni_{10-x}Co_x$ (x = 0, 1, 2, 3, 4), and for convenience, the alloys were denoted with Co content as Co_0, Co_1, Co_2, Co_3 and Co_4, respectively.

The phase structures and compositions of the as-cast and spun alloys were determined by XRD diffractometer (D/max/2400). The diffraction, with the experimental parameters of 160 mA, 40 kV and 10°/min, respectively, was performed with Cu $K_{\alpha 1}$ radiation filtered by graphite. The morphologies of the as-cast alloys were examined by scanning electronic microscope (SEM) (Philips QUANTA 400). The thin film samples of the as-spun alloys were prepared by ion etching for observing the morphology with high-resolution transmission electronic microscope (HRTEM) (JEM-2100F, operated at 200 kV), and for determining the crystalline state of the samples with electron diffraction (ED).

The differential scanning calorimetric (DSC) curves of the as-spun alloys were measured in argon flow to study their thermal stability.

The as-spun alloy ribbons were pulverized and then mixed with carbonyl nickel powder in a weight ratio of 1:4. The mixture was cold pressed at a pressure of 35 MPa into round electrode pellets of 15 mm in diameter and total mass of about 1 g. A tri-electrode open cell, consisting of a metal hydride electrode, a sintered $NiOOH/Ni(OH)_2$ counter electrode and an Hg/HgO reference electrode, was used for testing the electrochemical hydrogen storage characteristics of the experimental alloy electrodes. A 6 M KOH solution was used as electrolyte. The potential between the negative electrode and the reference electrode was defined as the discharge potential. In every cycle, the alloy electrode was first charged at a current density of 20 mA/g. After resting for 15 min, it was discharged at the same current density to cut-off potential of −0.500 V. The environment temperature of the measurement was kept at 30 °C.

3. Results and discussion

3.1. Microstructure characteristics

The XRD patterns of the as-cast and spun alloys were shown in Fig. 1. It can clearly be seen in Fig. 1 that no amorphous phase formed in the as-spun Co_0 alloy, but the as-spun Co_4 alloy showed the presence of an amorphous phase, and amorphized degree of the alloys significantly increases with rising spinning rate. Therefore, it can be concluded that the substitution of Co for Ni enhances the glass forming ability of the Mg_2Ni-type alloy. The impactful role of Co substitution on the glass forming ability was mainly attributed to fact that atomic radius of Co is larger than that of Ni. The glass forming ability of the alloy is closely relevant to the difference of the atom radius of the alloy. The bigger the difference of the atom radius, the higher the glass forming ability of the alloy [12]. It is also derived by comparing Fig. 1(a) with (b) that the substitution of Co for Ni did not change the major phase of the alloy, but it led to the formation of secondary phase $MgCo_2$. Listed in Table 1 were the lattice parameters, the cell volume and the full width at half maximum (FWHM) values of the main diffraction peaks of the as-cast and spun Co_0 and Co_4 alloys which were calculated by software of Jade 6.0. It can be derived from Table 1 that the substitution of Co for Ni caused the FWHM values of the main diffraction peaks of the as-cast and spun alloys significantly increased, and it led to the lattice parameters and cell volume of the alloys cleverly enlarged, which is attributed to the fact that the radius of Co atom is larger than that of Ni atom. It can also be seen in Table 1 that melt spinning produced broadened diffuse peaks, indicating refinement of the average grain size and stored stress in the grains.

The images of the as-cast Co_0 and Co_4 alloys taken by SEM were illustrated in Fig. 2, showing that the substitution of Co for Ni caused the grains of the as-cast alloy significantly refined, which is the reason why the substitution of Co for Ni leads to the main diffraction peaks of the alloys clearly broadened (Fig. 1). The morphology of the as-cast alloy changes from bulky dendrite structure to massive

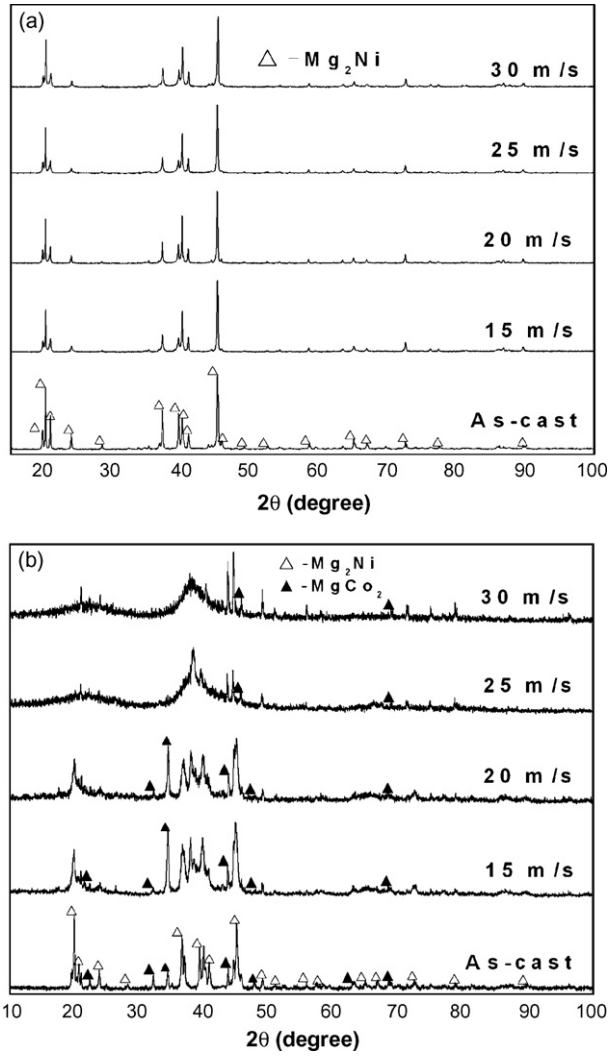

Fig. 1. X-ray diffraction patterns of the as-cast and spun alloys: (a) Co_0 alloy and (b) Co_4 alloy.

structure. The result obtained by energy dispersive spectrometry (EDS) indicates that the major phase of the Co_0 and Co_4 alloys is Mg_2Ni phase (denoted by A), but Co substitution leads to the secondary phase $MgCo_2$ formed (denoted by B), which is in agreement with the results of the XRD observation.

The morphologies of the as-spun (30 m/s) Co_0 and Co_4 alloys observed by HRTEM were shown in Fig. 3, showing that the as-spun Co_0 alloy displayed a nanocrystalline structure with grain size of about 30 nm, and its electron diffraction (ED) pattern appeared sharp multi-haloes, corresponding to a crystal structure. The morphologies of the as-spun Co_4 alloy exhibited a feature of the nanocrystalline with grain size of about 20 nm embedded in the amorphous matrix, and its electron diffraction pattern consisted of broad and dull halo, confirming the presence of an amorphous structure. This result agrees very well with the XRD observation shown in Fig. 1.

3.2. Thermal stability and crystallization

In order to examine the thermal stability and the crystallization of the as-spun amorphous and nanocrystalline/amorphous alloys, DSC analysis was conducted. The resulting profiles shown in Fig. 4 revealed that during heating the alloys crystallize completely, and the crystallization process of Co_4 alloy consists of two steps. The

Table 1
The lattice parameters, cell volume and the FWHM values of the diffraction peaks of the alloys.

Quenching rate (m/s)	FWHM values				Lattice parameters and cell volume					
	2θ (20.02°)		2θ (45.14°)		a (Å)		c (Å)		V (Å^3)	
	Co_0	Co_4	Co_0	Co_4	Co_0	Co_4	Co_0	Co_4	Co_0	Co_4
0	0.122	0.213	0.169	0.350	5.2097	5.2204	13.244	13.312	311.29	314.17
15	0.125	0.583	0.171	0.529	5.2099	5.2242	13.251	13.318	311.47	314.77
20	0.129	0.846	0.173	0.538	5.2101	5.2258	13.258	13.320	311.66	315.01
25	0.131	–	0.179	–	5.2105	–	13.265	–	311.83	–
30	0.133	–	0.181	–	5.2106	–	13.287	–	312.40	–

first crystallization reaction at about 232 °C is connected with a sharp exothermic DSC peak, followed by a smaller and wider peak (418 °C) corresponding to a second crystallization reaction. It was proved that the first sharper peak corresponds to the crystallization (ordering) of the amorphous into nanocrystalline Mg_2Ni [13].

3.3. Electrochemical performances

3.3.1. Activation capability and discharge capacity

The activation capability, which is a very important performance for the practical use of Ni–MH battery, was characterized by the number of charge–discharge required for attaining the greatest discharge capacity through a charge–discharge cycle at a constant current density. The fewer the cycle number, the better the activation performance. The cycle number dependence of the discharge capacity of the alloys was illustrated in Fig. 5, the charging–discharging current density being 20 mA/g. The figure showed that all the alloys had excellent activation capabilities and attained their maximum discharge capacities at first charging–discharging cycle. The melt spinning markedly enhanced the discharge capacity of the alloys. When the spinning rate increased from 0 to 30 m/s, the discharge capacity of the Co_0 alloy grew from 30.3 to 135.5 mAh/g, and from 113.3 to 402.5 mAh/g for Co_4 alloy. The nanocrystalline and amorphous microstructures formed by melt spinning are extremely helpful for enhancing hydrogen diffusivity and solubility, thus it sees to be self-evident that the discharge capacity of the alloys increases with rising spinning rate. It is noteworthy that, for a fixed spinning rate, the discharge capacity of the Co_4 alloy is much larger than that of Co_0 alloy, which is mainly ascribed to the fact that the substitution of Co for Ni enhances markedly the glass forming ability of the Mg_2Ni-type alloy owing to amorphous Mg_2Ni alloy showing a large discharge capacity.

Fig. 6 showed the influence of Co content on the discharge capacity of the as-cast and spun alloys, indicating that the substitution of Co for Ni significantly increased the discharge capacity of the as-cast and spun alloys. It is noteworthy that the influence of the substitution of Co for Ni on the discharge capacity of the as-spun alloy is much more significant than on that of the as-cast alloy. When Co content grew from 0 to 4, the maximum discharge capacity of the as-cast alloy increased from 30.3 to 113.3 mAh/g, and from 135.5 to 402.5 mAh/g for as-spun (30 m/s) alloy. Some explanations may be offered as the reason of which leads to about mentioned results. For the as-cast alloys, the substitution of Co

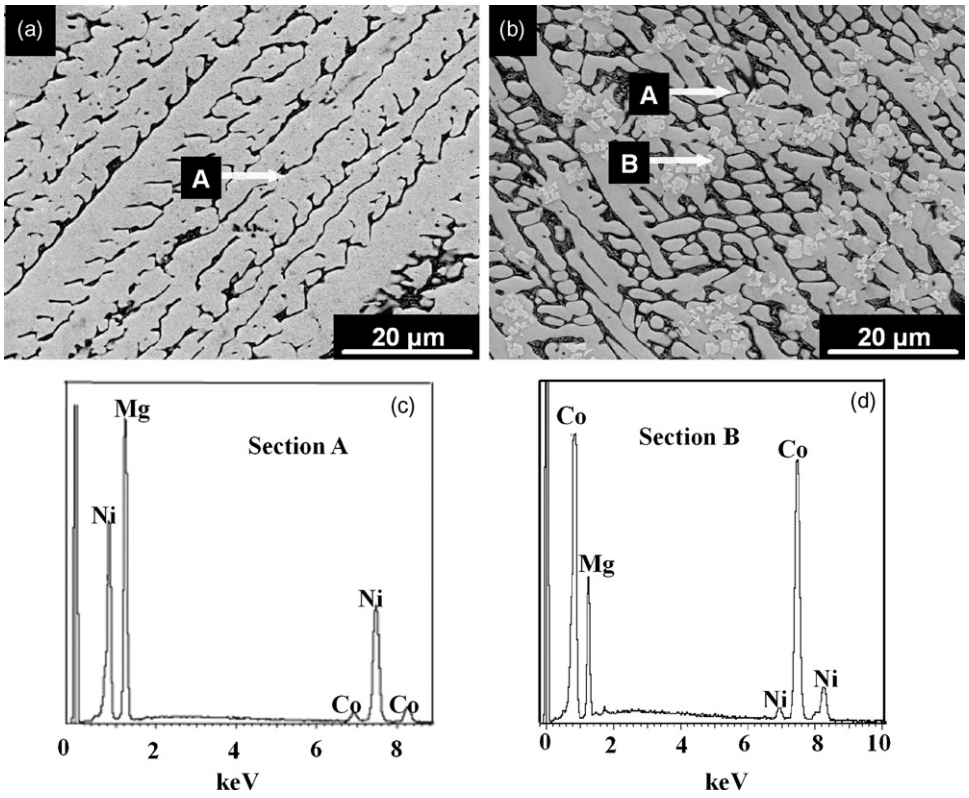

Fig. 2. The images of the Co_0 and Co_4 alloys taken by SEM together with typical EDS spectra of sections A and B in (b): (a) morphology of Co_0 alloy, (b) morphology of Co_4 alloy, and (c) EDS of section A and (D) EDS of section B.

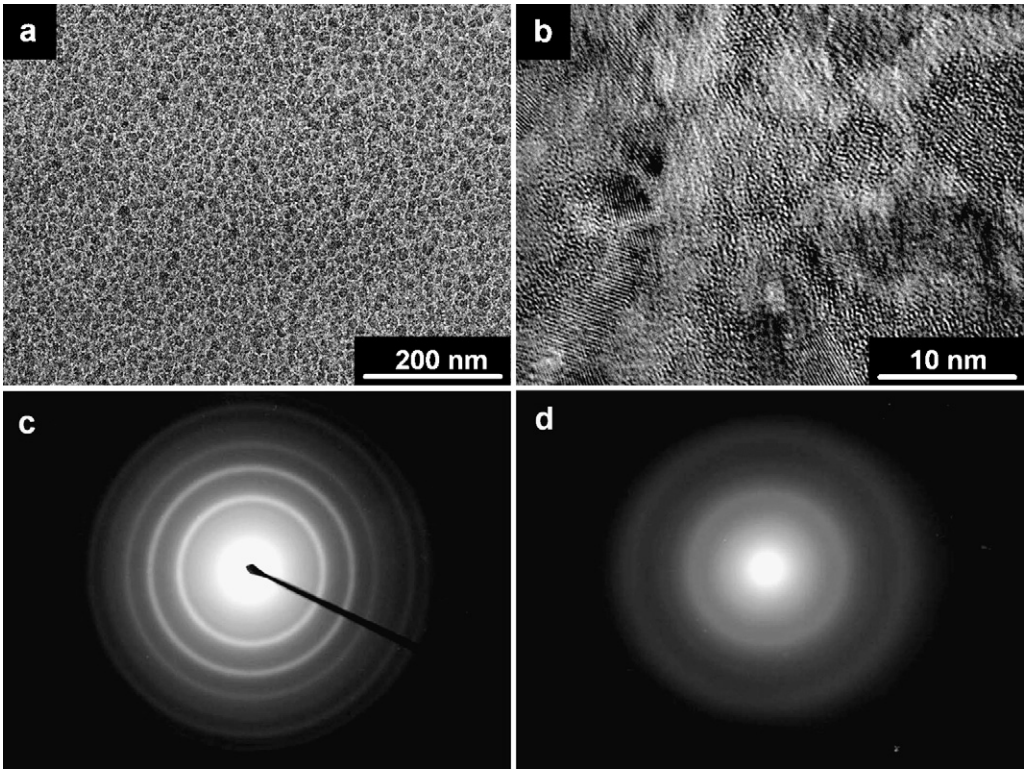

Fig. 3. Morphologies and ED of the as-spun alloys (30 m/s) taken by HRTEM: (a) morphology of Co_0 alloy, (b) morphology of Co_4 alloy, (c) ED of Co_0 alloy, and (d) ED of Co_4 alloy.

for Ni in Mg_2Ni compound decreases the stability of the hydride and makes the desorption reaction easier [14,15]. The secondary phase $MgCo_2$ probably worked as a catalyst to activate the Mg_2Ni phase to absorb/desorb reversibly hydrogen in the alkaline electrolyte. For the as-spun alloys, the increased discharge capacity is attributed to the enhanced the glass forming ability of the alloys by Co substitution. A proper ratio of amorphous and nanocrystalline provided an excellent discharge property of the Mg–Ni-based alloy [9]. Some reports on the hydriding/dehydriding properties of the amorphous phase are conflicting. Ryan et al. [16] reported that the discharge capacity of $Ni_{64}Zr_{36}$ amorphous alloys was 200 mAh/g for which the large reversible hydrogen solubility of the amorphous phase is responsible. Liu et al. [17] and Lee and Ha [18] confirmed the electrode capacity of Mg–Ni and Ti–Fe amorphous phases was greatly improved, since the diffusivity and solubility of hydrogen were larger in an amorphous phase than in a crystalline phase. Libowitz and Maeland [19] considered that the amount of absorbed hydrogen was larger in a crystalline phase than in an amorphous phase. Li and Cheng [20] confirmed that the discharge capacity of the La–Mg amorphous alloy is about half as large as that of the crystalline alloy. None of the theories can satisfactorily explain the above-mentioned experimental results. Authors considered that high-density crystal defects, nanocrystalline, especial an amorphous phase formed during melt spinning can significantly improve the electrocatalytic activity and dynamic performance of the hydrogen absorption/desorption of the Mg-based hydrogen storage alloys. Consequently, the Mg-based alloys with the amorphous structure have a large discharge capacity. But the amorphization does not enhance the latent capability of the hydrogen absorption of the Mg-based alloy because the practical discharge capacity of the homogeneous amorphous Mg_2Ni alloy still is much lower than its theoretical one.

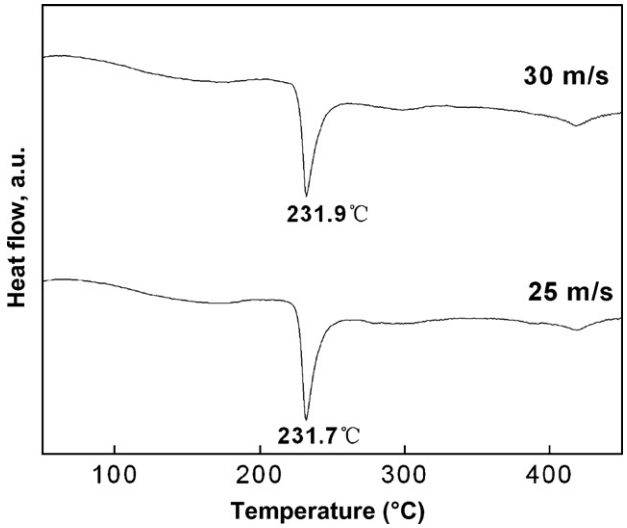

Fig. 4. DSC profiles of Co_4 alloy spun at 25 and 30 m/s.

3.3.2. Cycle stability

The capacity retaining rate (R_h), which was introduced to accurately evaluate the cycle stability of the alloy, is defined as $R_h = C_n/C_{max} \times 100\%$, where C_{max} is the maximum discharge capacity and C_n is the discharge capacity of the nth charge–discharge cycle, respectively. According to the above-mentioned definition, it can be known that the larger the capacity retaining rate (R_h), the better the cycle stability of the alloy.

The capacity retaining rates of the Co_0 and Co_4 alloys as functions of the cycle number were plotted in Fig. 7. The melt-spinning engendered a negligible influence on the capacity retaining rate of Co_0 alloy, and the capacity retaining rates of as-cast and spun Co_0 fell to around 30% after 20 cycles, meaning the Co_0 alloy possesses

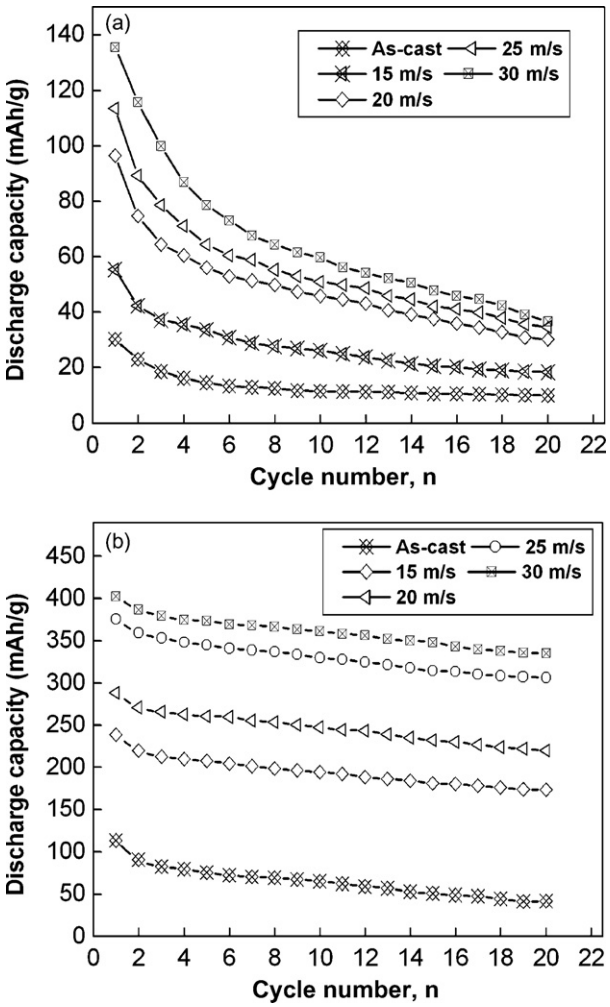

Fig. 5. Evolution of the discharge capacity of the as-cast and spun alloys with the cycle number: (a) Co_0 alloy and (b) Co_4 alloy.

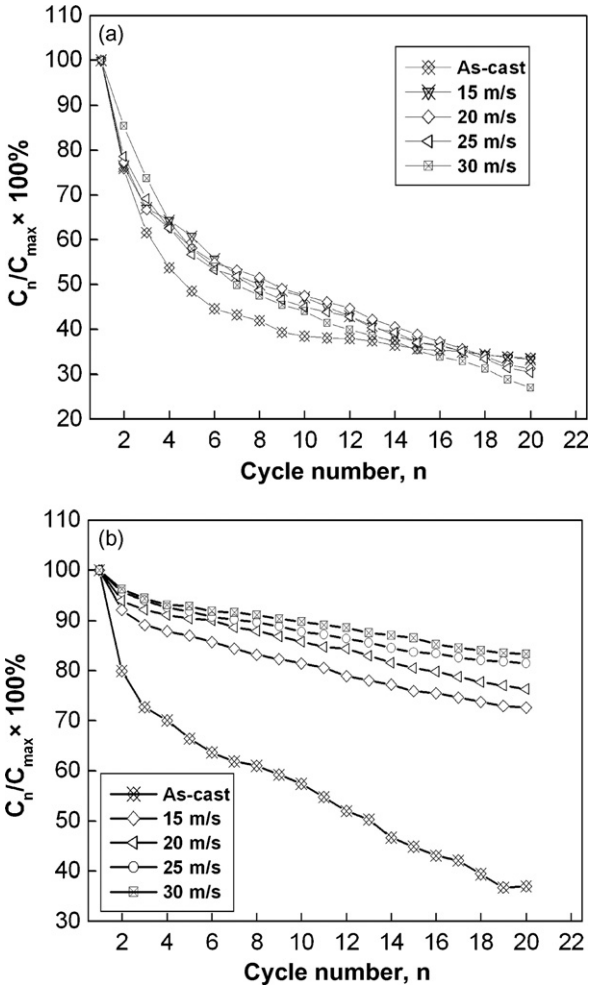

Fig. 7. Evolution of the capacity retaining rate of the as-spun alloys with cycle number: (a) Co_0 alloy and (b) Co_4 alloy.

poor cycle stability. Correspondingly, the melt spinning significantly enhanced the cycle stability of Co_4 alloy, for which the glass forming ability enhanced by Co substitution is mainly responsible. When spinning rate increased from 0 to 30 m/s, the capacity retaining rate of the Co_4 alloys after 20 cycles rose from 37.04 to 83.35%, but it declined from 33.54 to 27.05% for the Co_0 alloy, which was mainly attributed to the refined grain by melt spinning. It was well known that the essential reason of which leads to the loss efficacy of the Mg-based alloy electrodes is the severe corrosion of Mg in the alkaline KOH solution [21–23]. The grain refining consequentially weakens the anti-corrosion capability of the alloy due to the fact that intercrystalline corrosion is inevitable. Therefore, it is understandable why melt spinning slightly impairs the cycle stability of the Co_0 alloy. The melt spinning strongly heightened the cycle stability of the Co_4 alloy, which was mainly attributed to the formation of an amorphous phase.

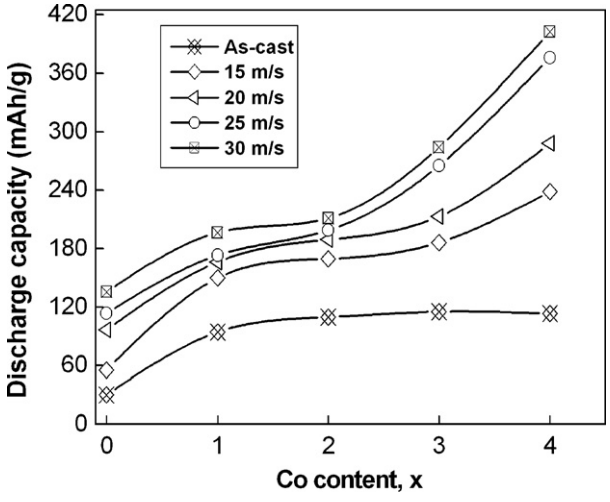

Fig. 6. Evolution of the maximum discharge capacity of the alloys with Co content.

The Co content dependence of the capacity retaining rates of the as-cast and spun alloys at 20th cycle was plotted in Fig. 8, showing that the substitution of Co for Ni significantly raises the capacity retaining rates of the alloy. The grain refinement is disadvantageous for improving anti-intercrystalline corrosion ability of the alloy. It is noteworthy that the substitution of Co for Ni significantly refined the grains of the as-cast alloy (Fig. 2) but the cycle stability of the as-cast alloy did not decrease with rising Co content. Obviously, it is ascribed to the fact that the decreased degree of the grain size of the as-cast alloy caused by Co substitution is much smaller than that produced by melt spinning. The positive impact of Co substitution on the cycle stability of the alloy was ascribed to two reasons. One is that the enlarged cell volume caused by Co substitution decreased the ratios of expansion/contraction of the alloys in process of the hydrogen absorption/desorption, which means increasing the anti-pulverization capability of the alloy. On the other hand, the glass forming ability enhanced by Co substitution is extremely important

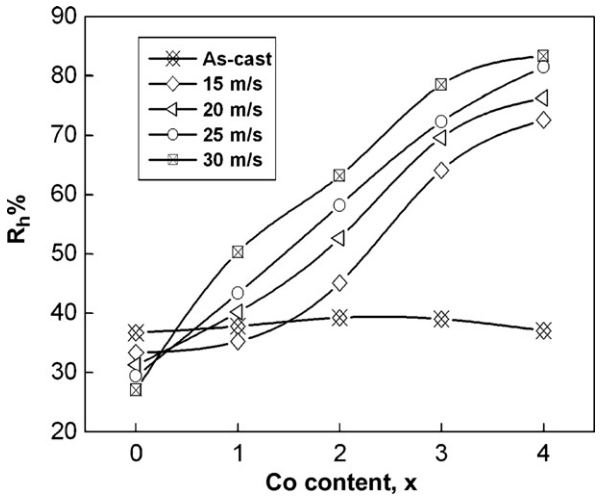

Fig. 8. Evolution of the capacity retaining rate at 20th cycle with Co content.

because an amorphous phase improves not only anti-pulverization ability but also anti-corrosion and anti-oxidation abilities of the alloy electrode in a corrosive electrolyte [24]. Based on the above-mentioned results, it can be concluded that an impactful approach for improving the cycle stability of the Mg-based alloy electrodes is to intensify its anti-corrosion and anti-oxidation capabilities.

4. Conclusions

1. The investigation on the structures of the as-cast and spun $Mg_{20}Ni_{10-x}Co_x$ (x = 0, 1, 2, 3, 4) alloys showed that the substitution of Co for Ni significantly enhanced the glass forming ability of Mg_2Ni-type alloy and led to the grains of the as-cast alloy markedly refined. The substitution of Co for Ni did not change the major phase of Mg_2Ni in the alloy, but it caused the formation of the secondary phase $MgCo_2$.
2. The substitution of Co for Ni significantly improved the electrochemical hydrogen storage performances of the alloy, involving the discharge capacity and the cycle stability, which is mainly attributed to the enlarged cell volume, the refined grain, the decreased stability of the hydride and enhanced the glass forming ability produced by Co substitution.
3. Melt spinning significantly enhanced the discharge capacity and the cycle stability of the alloy containing Co, but its influence on the electrochemical performances of the Co-free alloy is insignificant, for which the difference of the glass forming ability of the alloys is mainly responsible.

Acknowledgements

This work is supported by Hi-Tech Research and Development Program of China (2006AA05Z132), National Natural Science Foundations of China (50871050), Natural Science Foundation of Inner Mongolia, China (200711020703) and Higher Education Science Research Project of Inner Mongolia, China (NJzy08071).

References

[1] J.H. Woo, K.S. Lee, J. Electrochem. Soc. 146 (3) (1999) 819–823.
[2] F.J. Liu, S. Suda, J. Alloys Compd. 231 (1995) 742–750.
[3] W.H. Liu, Y.Q. Lei, J. Wu, Q.D. Wang, Int. J. Hydrogen Energy 22 (1997) 999–1004.
[4] Y.Q. Lei, Y.M. Wu, Q.M. Yang, J. Wu, Q.D. Wang, Z. Phys. Chem. Bd. 183 (1994) 379–384.
[5] C. Iwakura, S. Nohara, H. Inoue, Y. Fukumoto, Chem. Commun. 15 (1996) 1831–1832.
[6] T. Kohno, M. Kanda, J. Electrochem. Soc. 144 (1997) 2384–2388.
[7] S. Nohara, N. Fujita, S.G. Zhang, H. Inoue, C. Iwakura, J. Alloys Compd. 267 (1998) 76–78.
[8] H. Kimura, T. Masumoto, Scripta Metall. 9 (1975) 211–222.
[9] L.J. Huang, G.Y. Liang, Z.B. Sun, D.C. Wu, J. Power Sources 160 (2006) 684–687.
[10] T. Spassov, U. Köster, J. Alloys Compd. 287 (1999) 243–250.
[11] S.I. Yamaura, H.Y. Kim, H. Kimura, A. Inoue, Y. Arata, J. Alloys Compd. 339 (2002) 230–235.
[12] H.S. Chen, Acta Met. 22 (12) (1974) 1505–1511.
[13] T. Spassov, P. Solsona, S. Suriñach, M.D. Barô, J. Alloys Compd. 349 (2003) 242–254.
[14] J.H. Woo, K.S. Lee, J. Electrochem. Soc. 146 (1999) 819–823.
[15] Y. Takahashi, H. Yukawa, M. Morinaga, J. Alloys Compd. 242 (1996) 98–107.
[16] D.H. Ryan, F. Dumais, B. Patel, J. Kycia, J.O. Strom-Olsen, J. Less-Common Met. 172–174 (1991) 1251–1296.
[17] W. Liu, Y. Lei, D. Sun, J. Wu, Q. Wang, J. Power Sources 58 (1996) 243–247.
[18] K.S. Lee, C.J. Ha, Kor. J. Mater. Res. 5 (1) (1995) 112–120.
[19] G.G. Libowitz, A.J. Maeland, J. Less-Common Met. 101 (1984) 131–143.
[20] Y. Li, Y.T. Cheng, J. Alloys Compd. 223 (1995) 6–12.
[21] N.H. Goo, J.H. Woo, K.S. Lee, J. Alloys Compd. 288 (1999) 286–293.
[22] L.B. Wang, Y.H. Tang, Y.J. Wang, Q.D. Li, H.N. Song, H.B. Yang, J. Alloys Compd. 336 (2002) 297–300.
[23] J.J. Jiang, M. Gasik, J. Power Sources 89 (2000) 117–124.
[24] Y.H. Zhang, B.W. Li, H.P. Ren, Y. Cai, X.P. Dong, X.L. Wang, Int. J. Hydrogen Energy 32 (2007) 4627–4634.